Representation of videokeratoscopic height data with Zernike polynomials

Jim Schwiegerling

Optical Sciences Center, University of Arizona, Tucson, Arizona 85721

John E. Greivenkamp and Joseph M. Miller

Optical Sciences Center and Department of Ophthalmology, University of Arizona, Tucson, Arizona 85721

Received November 23, 1994; revised manuscript received April 17, 1995; accepted May 15, 1995

Videokeratoscopic data are generally displayed as a color-coded map of corneal refractive power, corneal curvature, or surface height. Although the merits of the refractive power and curvature methods have been extensively debated, the display of corneal surface height demands further investigation. A significant drawback to viewing corneal surface height is that the spherical and cylindrical components of the cornea obscure small variations in the surface. To overcome this drawback, a methodology for decomposing corneal height data into a unique set of Zernike polynomials is presented. Repeatedly removing the low-order Zernike terms reveals the hidden height variations. Examples of the decomposition-and-display technique are shown for cases of astigmatism, keratoconus, and radial keratotomy. © 1995 Optical Society of America

1. INTRODUCTION

Use of commercially available videokeratoscopes by eye-care providers and vision scientists has become widespread. The majority of these devices are based upon Placido-disk technology, in which a series of concentric illuminated rings (mires) reflect off the cornea of an observer and are imaged, along with the cornea, by a video camera. From knowledge of the geometry of the keratoscope and the variations in ring spacing in the image, the slope of the corneal surface can be determined in the meridional direction. For display and analysis of the data obtained from videokeratoscopes, the corneal slope data are usually converted to a more intuitive form. The derivative of the acquired slope data gives corneal curvature and is related to the optical power of the surface. There are some ambiguities associated with this technique that stem mainly from alternative definitions of curvature and power. The accuracy and validity of these definitions have been extensively debated, and a thorough analysis is given by Roberts.[1] The corneal slope data can also be integrated for determining the height or sag of the corneal surface. This method has the advantage that the true topography of the cornea is given. However, higher-order height variations tend to be concealed by the lower-order components of the cornea. Examples of interpreting videokeratographic height data are given by several authors.[2–6]

The most common method for displaying videokeratoscopic data is a color-coded map that gives some measure of the dioptric power distribution of the cornea. For these displays, the corneal slope data are used to calculate the axial or instantaneous curvature at a given point on the cornea. By assuming an effective index of the cornea, one can calculate a local dioptric power from the curvature data. These maps use a color scale on which each color corresponds to a range of power, so that the power map is a contour plot of corneal dioptric power. Recently, however, cases for using curvature maps and height maps as alternatives or complements to power maps have been made. Eye-care providers and vision scientists use videokeratographic data for a variety of applications, and a given display method may prove more beneficial depending on the application. The corneal curvature map may be advantageous to the optometrist fitting contacts or spectacles. The refractive surgeon may wish to examine changes in dioptric power resulting from surgery. The optical engineer may prefer a height map of the cornea in order to determine the optical quality of the surface and model the effects of various corneal conditions. Regardless of the application, a thorough understanding of the benefits and drawbacks of each method is necessary to enable one to choose the appropriate analysis and display method for the appropriate application.

In this paper a methodology for analyzing videokeratographic height data is presented. The technique involves decomposing the corneal height data in terms of the orthonormal set of Zernike polynomials. The use of Zernike polynomials to represent the corneal surface has been suggested by several authors.[2–6] This is a direct analogy to the widespread use of Zernike polynomials in the optical fabrication and testing area.[7–9] We have also been told that this feature is an unpublished capability of a prototype corneal topographer.[10] Once the Zernike polynomial decomposition is complete, the fundamental components of the corneal surface are related to more-familiar quantities such as spherical and cylindrical curvature and power. A drawback to viewing the videokeratographic height data is that the fine variations in corneal height are obscured by the spherical and cylindrical components of the cornea. In order to visualize these residual higher-order height variations of the cornea, we subtract the lower-order components from the original height data. In this paper this decomposition-

0740-3232/95/102105-09$06.00

and-display technique is applied to topographies of an eye with regular corneal astigmatism, an eye diagnosed with advanced keratoconus, and two eyes that underwent radial keratotomy. Advantages of this technique over previous efforts and its accuracy and limitations are discussed.

2. DECOMPOSITION OF SURFACES

The shape of a surface is represented mathematically as a function of two variables. In a Cartesian coordinate system this function has the form $z = f(x, y)$, where z is the height or sag of the surface at a given point (x, y). When the functional form of $f(x, y)$ is complicated, analysis of the surface is sometimes simplified by representation of the surface as a linear combination of simpler surfaces. These simpler surfaces are described mathematically by the set of functions $\{g_j(x, y)\}$ and are combined such that

$$f(x, y) \cong \sum_{j=1}^{\infty} a_j g_j(x, y), \tag{1}$$

where a_j is a constant describing the weighting on each function $g_j(x, y)$.[11,12]

The set of functions $\{g_j(x, y)\}$ is said to be complete if any arbitrary square-integrable function $f(x, y)$ is exactly represented by the linear combination in relation (1). The most commonly used set of complete functions is $\{x^m y^n\}$, where m and n are positive integers. Relation (1) in this case becomes

$$f(x, y) = a_1 + a_2 x + a_3 y + a_4 x^2 + a_5 y^2 + a_6 xy + \ldots, \tag{2}$$

or the Taylor series expansion of $f(x, y)$ in two dimensions. The set of coefficients $\{a_j\}$ in relation (1) is usually found by the method of least squares. This technique minimizes the square of the difference between $f(x, y)$ and the series expansion, and this difference approaches zero as the number of terms in the series approaches infinity.

A set of complete functions $\{g_j(x, y)\}$ is said to be orthonormal over a region A if they satisfy

$$\int_A g_j(x, y) g_k(x, y) \mathrm{d}x\mathrm{d}y = \begin{cases} 0 & \text{for } j \neq k \\ 1 & \text{for } j = k \end{cases}. \tag{3}$$

The Fourier series, a commonly used expansion for periodic functions, uses the complete orthonormal set of sinusoidal functions. The polynomials in the Taylor series expansion of Eq. (2), however, do not satisfy the orthogonality conditions of Eq. (3).

A simple method for determining the set of expansion coefficients $\{a_j\}$ exists when the functions $\{g_j(x, y)\}$ are orthonormal over a region A. If both sides of relation (1) are multiplied by $g_k(x, y)$ and integrated over the region A, then utilizing Eq. (3) yields

$$a_j = \int_A g_j(x, y) f(x, y) \mathrm{d}x\mathrm{d}y. \tag{4}$$

Equation (4) illustrates a significant advantage of orthonormal decomposition of surfaces over the least-squares method with use of nonorthonormal functions. Each of the coefficients a_j in Eq. (4) depends only on its corresponding function $g_j(x, y)$ and the original function. This relationship indicates that the set of coefficients $\{a_j\}$ are independent of one another and independent of the number of terms taken in the series expansion. In other words, the coefficients do not need to be recalculated when a more exact fit of $f(x, y)$ is desired. If, however, the set of functions $\{g_j(x, y)\}$ are not orthonormal, then the set of coefficients $\{a_j\}$ are interrelated. Each coefficient a_j depends on the entire set $\{g_j(x, y)\}$ and changes every time terms are added to the series expansion.

3. ZERNIKE POLYNOMIALS

The Zernike polynomials are a set of functions $\{Z_n^{\pm m}(\rho, \theta)\}$ that are orthonormal over the continuous unit circle.[6–9] They have been used extensively for phase-contrast microscopy, optical aberration theory, and interferometric testing to fit wave-front data. These functions are characterized by a polynomial variation in the radial direction ρ (for $0 \leq \rho \leq 1$) and a sinusoidal variation in the azimuthal direction θ. The polynomials are defined mathematically by

$$Z_n^{\pm m} = \begin{cases} \sqrt{2(n+1)}\, R_n^m(\rho) \cos m\theta & \text{for } +m \\ \sqrt{2(n+1)}\, R_n^m(\rho) \sin m\theta & \text{for } -m \\ \sqrt{(n+1)}\, R_n^m(\rho) & \text{for } m = 0 \end{cases}, \tag{5}$$

where

$$R_n^m(\rho) = \sum_{s=0}^{(n-m)/2} \frac{(-1)^s (n-s)!}{s!\left[\frac{(n+m)}{2} - s\right]!\left[\frac{(n-m)}{2} - s\right]!} \rho^{n-2s}, \tag{6}$$

n is the order of the polynomial in the radial direction ρ, and m is the frequency in the azimuthal direction θ. Several numbering systems are used for the Zernike terms; we have chosen the numbering system that is in the proposed ISO standards for optical components (ISO-10110).[13] The first six Zernike polynomials are given by

$$Z_0^0(\rho, \theta) = 1, \tag{7}$$

$$Z_1^1(\rho, \theta) = 2\rho \cos\theta, \tag{8}$$

$$Z_1^{-1}(\rho, \theta) = 2\rho \sin\theta, \tag{9}$$

$$Z_2^0(\rho, \theta) = \sqrt{3}(2\rho^2 - 1), \tag{10}$$

$$Z_2^2(\rho, \theta) = \sqrt{6}\rho^2 \cos 2\theta, \tag{11}$$

$$Z_2^{-2}(\rho, \theta) = \sqrt{6}\rho^2 \sin 2\theta. \tag{12}$$

Figure 1 shows several of these functions. The function Z_0^0 in Fig. 1(a) describes a surface of constant height. When a function is decomposed into Zernike polynomials, the coefficient of Z_0^0 is the mean height of the surface. When higher-order polynomials are added to the expansion, each term must have zero mean in order to satisfy the orthonormality condition of Eq. (3) and to leave the mean height of the fitted surface unchanged. Figures 1(b)–(d) show several of the zero-mean higher-order terms.

Another interesting property of the Zernike expansion is the redundant nature of the nonrotationally symmetric functions such as Z_1^1 and Z_1^{-1} or Z_2^2 and Z_2^{-2}. For

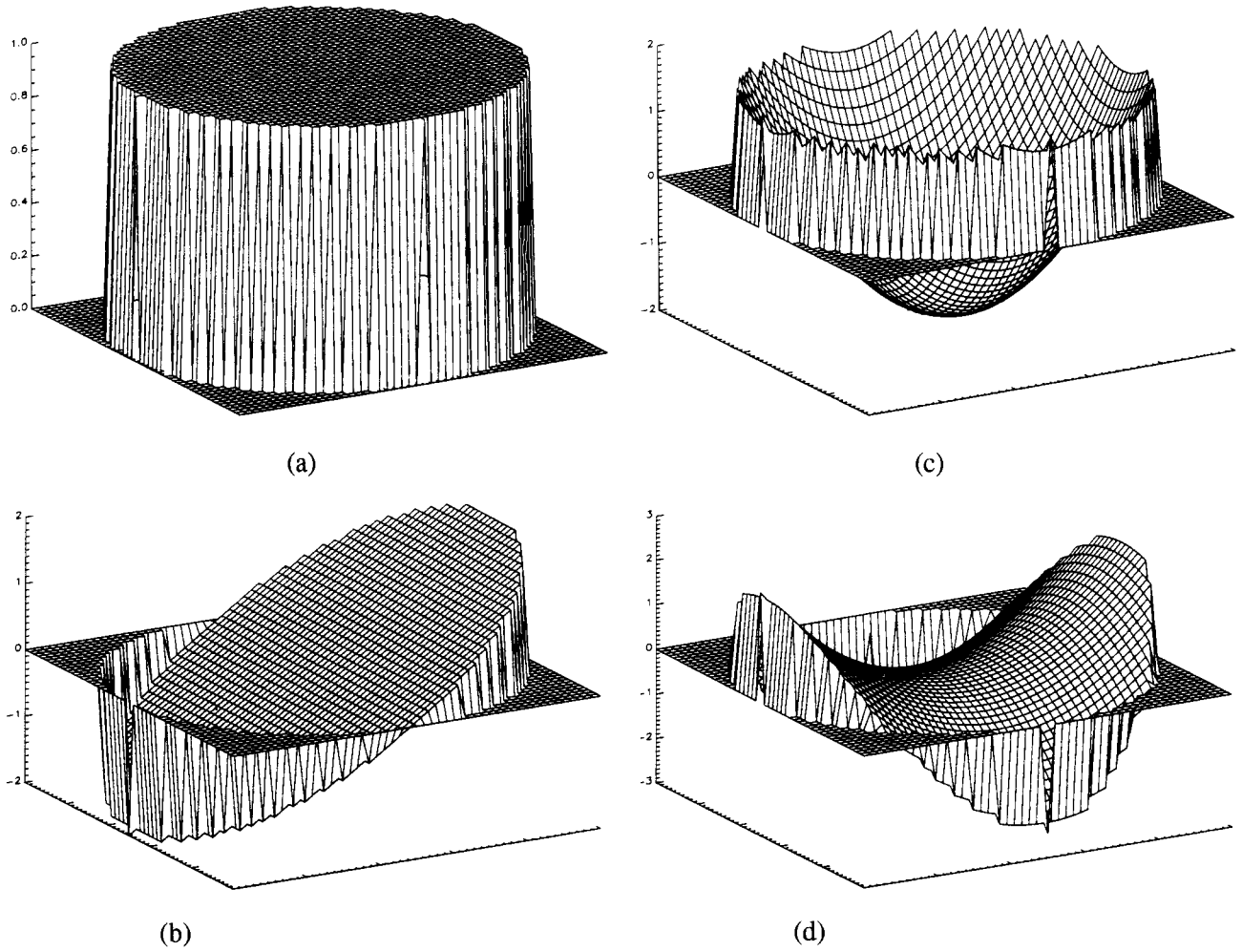

Fig. 1. Zernike polynomials: (a) Z_0^0, (b) Z_1^1 (Z_1^{-1} is the same as Z_1^1 but rotated 90°), (c) Z_2^0, (d) Z_2^{-2} (Z_2^2 is the same as Z_2^{-2} but rotated 45°).

instance, the function Z_1^1 describes a plane tilted about the y axis, and Z_1^{-1} similarly describes a plane tilted about the x axis (or Z_1^1 rotated 90°). If a plane tilted about an axis making an angle θ_0 relative to the y axis is expanded into Zernike polynomials, the coefficients Z_1^1 and Z_1^{-1} are appropriately weighted such that the ratio of their coefficients equals $\tan \theta_0$. This relationship, where one Zernike polynomial describes a surface and another describes a rotated version of the same surface, recurs throughout the set of Zernike polynomials. This feature allows the Zernike expansion to match a surface oriented at any angle.

Several of the low-order Zernike terms represent familiar corneal shapes. The Z_2^0 term in Fig. 1(c) is a paraboloid and represents an average curvature of the cornea. The functions Z_2^2 and Z_2^{-2} in Fig. 1(d), which describe corneal astigmatism, are two saddle-shaped surfaces rotated 45° with respect to each other. When the saddle shape of the Z_2^2 and Z_2^{-2} terms is added to the paraboloid described by Z_2^0, the radius of curvature of the paraboloid is shortened along one axis and lengthened along a perpendicular axis. The longer radius of curvature defines the base sphere of the cornea, and the difference between the radii of curvature defines the cylindrical component of the cornea (in plus-cylinder form). The astigmatic axis is given by the orientation of the saddle surface formed by the sum of the Z_2^2 and Z_2^{-2} terms.

Since the Zernike polynomials are orthogonal over the continuous unit circle and the lower-order terms represent familiar corneal shapes such as sphere and cylinder, the Zernike polynomials appear to be an ideal set of functions for decomposing and analyzing corneal surface height. Videokeratoscopes, however, measure the corneal height only at a discrete number of points, and unfortunately the Zernike polynomials are not orthogonal over a discrete set of points. A technique known as Gram–Schmidt orthogonalization, however, allows the discrete set of corneal height data to be expanded in terms of the Zernike polynomials and still keep the advantages of an orthogonal expansion.

The procedure for Gram–Schmidt orthogonalization is outlined by Wang and Silva[9] (with one minor correction noted after the Ref. 9 entry in the References) and is not repeated here. The basic premise of the orthogonalization routine is that the Zernike polynomials are not orthogonal over a discrete set of points, or

$$\sum_i Z_n^{\pm m}(\rho_i, \theta_i) Z_{n'}^{\pm m'}(\rho_i, \theta_i) \neq \delta_{nn'}\delta_{mm'}, \tag{13}$$

for all discrete points (ρ_i, θ_i). By taking various linear

combinations of the Zernike functions, however, one can construct a new set of functions $U_n^{\pm m}(\rho_i, \theta_i)$ such that

$$U_n^{\pm m}(\rho_i, \theta_i) = \sum_{n',\pm m'}^{n,\pm m} b_{n,\pm m,n',\pm m'} Z_{n'}^{\pm m'}(\rho_i, \theta_i). \quad (14)$$

Through the appropriate choice of the coefficients $b_{n,\pm m,n',\pm m'}$, the functions $U_n^{\pm m}(\rho_i, \theta_i)$ can be made orthogonal, or

$$\sum_i U_n^{\pm m}(\rho_i, \theta_i) U_{n'}^{\pm m'}(\rho_i, \theta_i) = \delta_{nn'}\delta_{mm'}. \quad (15)$$

The corneal height data are decomposed into a linear combination of the functions $U_n^{\pm m}(\rho_i, \theta_i)$. The expansion coefficients for these new functions are given by Eq. (4); however, the integral collapses to a sum because of the discrete number of points. Once the expansion is complete, the orthogonal functions are converted back into terms of the Zernike polynomials. The result is a unique set of Zernike coefficients.

4. DECOMPOSITION AND DISPLAY OF REAL TOPOGRAPHY DATA

The decomposition techniques outlined above were used to analyze real corneal height data taken from a Computed Anatomy TMS-1 videokeratoscope (New York, N.Y.). The corneal height data $f(r_i, \theta_i)$ and a set of radial coordinates r_i are provided as direct output of the TMS-1. Since the TMS-1 uses continuous mires, no information about azimuthal coordinates is obtained. The azimuthal coordinates θ_i are therefore assumed to be 256 uniformly spaced sectors on a polar grid. The effects of this approximation are discussed in more detail in Section 5. Since the Zernike polynomials are orthonormal only over the unit circle, the radial coordinates r_i need to be normalized by the maximum radial extent of the data $r_{\max}$ such that $\rho_i = r_i/r_{\max}$.

The discrete set of data points are expanded into Zernike polynomials by use of the Gram–Schmidt orthogonalization procedure outlined above, such that

$$f(\rho_i, \theta_i) = \sum_{n,\pm m} a_{n,\pm m} Z_n^{\pm m}(\rho_i, \theta_i), \quad (16)$$

for all points (ρ_i, θ_i). From the set of coefficients $\{a_{n,\pm m}\}$, values for the base and the astigmatic radii of curvature and power, as well as for the cylinder axis, can be calculated.

For determining the spherical and cylindrical components of the series expansion, the cylindrical axis needs to be found. This axis is defined by the lowest-order astigmatic terms of the expansion. These astigmatic terms are given by

$$\sqrt{6}\, a_{2,-2}\rho^2 \sin(2\theta) + \sqrt{6}\, a_{2,2}\rho^2 \cos(2\theta). \quad (17)$$

By taking the derivative of this expression with respect to θ and finding the extremum,

$$a_{2,-2}\cos(2\theta) - a_{2,2}\sin(2\theta) = 0. \quad (18)$$

If the axis θ_0 is defined as

$$\theta_0 = \frac{1}{2}\tan^{-1}\left(\frac{a_{2,-2}}{a_{2,2}}\right), \quad (19)$$

then two relevant solutions exist for Eq. (18). These solutions are $\theta = \theta_0$ and $\theta = \theta_0 + 90°$. The astigmatic axis is given by

$$\theta_a = \begin{cases} \theta_0 & \text{for } a_{2,-2}\sin 2\theta_0 + a_{2,2}\cos 2\theta_0 < 0 \\ \theta_0 + 90° & \text{for } a_{2,-2}\sin 2\theta_0 + a_{2,2}\cos 2\theta_0 > 0 \end{cases}. \quad (20)$$

If θ_a is negative then add 180°, so that θ_a always lies in the range $0 \le \theta_a < 180°$. For the base spherical and cylindrical powers to be determined, the radii of curvature along θ_0 and the axis perpendicular to it need to be determined.

The parabolic terms of the expansion oriented along θ_0 can be used as an approximation to the spherical and cylindrical components of $f(r_i, \theta_i)$. The Zernike polynomials with even radial order $n \ge 2$ and azimuthal frequencies $m = 0$ or $m = \pm 2$ all contain a parabolic term. The first six of these polynomials are

$$Z_2^0(\rho, \theta) = \sqrt{3}(2\rho^2 - 1), \quad (21)$$

$$Z_2^2(\rho, \theta) = \sqrt{6}\,\rho^2 \cos 2\theta, \quad (22)$$

$$Z_2^{-2}(\rho, \theta) = \sqrt{6}\,\rho^2 \sin 2\theta, \quad (23)$$

$$Z_4^0(\rho, \theta) = \sqrt{5}(6\rho^4 - 6\rho^2 + 1), \quad (24)$$

$$Z_4^2(\rho, \theta) = \sqrt{10}(4\rho^2 - 3)\rho^2 \cos 2\theta, \quad (25)$$

$$Z_4^{-2}(\rho, \theta) = \sqrt{10}(4\rho^2 - 3)\rho^2 \sin 2\theta. \quad (26)$$

For obtaining the spherical and cylindrical components of the corneal height data, the parabolic terms of the Zernike expansion are compared with a paraboloid of the form

$$\text{sag} = \frac{r^2}{2R_0} = \frac{\rho^2 r_{\max}^2}{2R_0}, \quad (27)$$

where r is the radial coordinate and R_0 is the radius of curvature of the paraboloid. This value R_0 is used as an approximation of the radius of curvature of the corneal surface. The radius of curvature in general will differ along the axes of the cornea as a result of astigmatism. Therefore define $R_0 = R_\perp$ for $\theta = \theta_0$, and define $R_0 = R$ for $\theta = \theta_0 + 90°$. Equating the Zernike expansion terms containing ρ^2 oriented along θ_0 with Eq. (27) yields

$$\begin{aligned} \frac{\rho^2 r_{\max}^2}{2R_\perp} = {} & 2\sqrt{3}\,a_{2,0}\rho^2 + \sqrt{6}\,a_{2,2}\rho^2 \cos 2\theta_0 \\ & + \sqrt{6}\,a_{2,-2}\rho^2 \sin 2\theta_0 - 6\sqrt{5}\,a_{4,0}\rho^2 \\ & - 3\sqrt{10}\,a_{4,2}\rho^2 \cos 2\theta_0 \\ & - 3\sqrt{10}\,a_{4,-2}\rho^2 \sin 2\theta_0 + \ldots. \end{aligned} \quad (28)$$

Solving for $R_\perp$ and truncating higher-order terms, we obtain

$$R_\perp = \frac{r_{\max}^2}{2[2\sqrt{3}\,a_{2,0} - 6\sqrt{5}\,a_{4,0} + \sqrt{6}(a_{2,2}\cos 2\theta_0 + a_{2,-2}\sin 2\theta_0) - 3\sqrt{10}(a_{4,2}\cos 2\theta_0 + a_{4,-2}\sin 2\theta_0)]}. \quad (29)$$

If $R_\perp$ is in millimeters, the power $\Phi_\perp$ along $\theta = \theta_0$ in

diopters is given by

$$\Phi_{\perp} = 1000\,\frac{n-1}{R_{\perp}}, \tag{30}$$

where n is usually 1.3375.

Similarly, for $\theta = \theta_0 + 90°$,

$$R = \frac{{r_{\max}}^2}{2[2\sqrt{3}\,a_{2,0} - 6\sqrt{5}\,a_{4,0} - \sqrt{6}\,(a_{2,2}\cos 2\theta_0 + a_{2,-2}\sin 2\theta_0) + 3\sqrt{10}(a_{4,2}\cos 2\theta_0 + a_{4,-2}\sin 2\theta_0)]}, \tag{31}$$

and the power Φ along $\theta = \theta_0 + 90°$ in diopters is given by

$$\Phi = 1000\,\frac{n-1}{R}, \tag{32}$$

where n is usually 1.3375.

The cylindrical power Φ_a is diopters is therefore given by

$$\Phi_a = \Phi_{\perp} - \Phi\,. \tag{33}$$

These results can be expressed in the familiar plus-cylinder form ($\Phi + \Phi_a \times \theta_a$).

Equations (29)–(33) display one of the drawbacks to using Zernike polynomials. For determining the radii of curvature along the principal meridians, an infinite number of Zernike coefficients are needed. The radii-of-curvature equations above have been truncated so that they contain only the first six Zernike terms with parabolic dependence. However, the values for the radii of curvature converge quickly, so that the truncation error becomes small. The accuracy of these equations is discussed in greater detail in Section 5. A second drawback is that the value of $r_{\max}$ can change from data set to data set. The values of the expansion coefficients cannot be directly compared between two decompositions unless the values of $r_{\max}$ are equal.

When one is viewing corneal height data, fine height variations in the corneal surface are obscured by the base spherical and cylindrical components. The decomposition technique allows a simple method for displaying some of these higher-order variations. Repeatedly removing lower-order expansion terms causes the higher-order variations to become increasingly apparent. For example, to permit astigmatism to be seen more clearly, the parabolic term is subtracted from the original height data. For higher-order height variations to be seen, the astigmatic component of the corneal surface is subtracted. In some cases, as will be seen below, removing additional terms will reveal additional interesting corneal height artifacts.

The corneal height maps take on characteristics different from those of the more-familiar power map distributions. These differences may initially prove confusing to the viewer who is used to seeing corneal power displays. The novice viewer must remember that the height map displays the sag of the corneal surface as opposed to surface curvature or power. The uniform power map distribution associated with spherical surfaces (under one definition of power) is seen as a central peak falling off evenly in all radial directions in a height map. The familiar "bow-tie" pattern seen in an astigmatic power map is seen as a saddle shape in the height map. Interpreting height maps requires only a modest amount of reeducation on the part of the new viewer. The technique of removing low-order terms from the original corneal height data can be thought of as a generalization of fluorescein maps. For fluorescein maps, a spherical term is removed from the corneal height data by means of a contact lens, resulting in a display of the residual height variation. For the Zernike decomposition technique, more-complex shapes are removed to reveal the residual corneal height data.

Figures 2 through 5 show several examples of the decomposition-and-display technique. Each of the figures displays a gray-scale height map of the cornea and notes the range of heights. The patient whose data are displayed in Fig. 2 has corneal astigmatism. Figure 2(a) shows the raw height data obtained from the TMS-1. In Fig. 2(b) the parabolic component Z_2^0 of the original height data has been removed. The astigmatism (saddle shape) in the resultant display is apparent. In Fig. 2(c) the cylindrical terms Z_2^{-2} and Z_2^2 have been removed to reveal the residual higher-order variations in the cornea. The prescription for spherical power and astigmatism predicted by Eqs. (16)–(22) is 46.9 D + 2.1 D × 1° compared with a Sim K value of 48.9 D × 86°/46.9 D × 176° and a Min K value of 46.8 D × 1° determined by the TMS-1. The Sim K value finds the maximum power along a meridian in the paraxial region of the cornea and gives this power, its orientation, and the corneal power in a perpendicular meridian. The Min K similarly finds the minimum power along a meridian in the paraxial region and gives its magnitude and orientation. The data displayed in Fig. 3 are for the patient who has been diagnosed with advanced keratoconus. Figure 3(a) once again shows the raw topography height data. In Fig. 3(b) the base curvature has been subtracted. In Fig. 3(c) the cylindrical terms Z_2^{-2} and Z_2^2 have been removed to reveal the cone.

The patients whose data are displayed in Figs. 4 and 5 have undergone six- and eight-incision radial keratotomy, respectively. Figures 4(a) and 5(a) once again show the raw topography height data. In Figs. 4(b) and 5(b) the base curvature has been subtracted. In Fig. 4(c) terms of the Zernike expansion with radial order $n \leq 6$ and azimuthal frequency $m < 6$ have been subtracted from the original height data, revealing the height variations resulting from the six RK incisions. Only these Zernike terms are removed from the six-incision RK, because some of the higher terms contain a sixfold symmetry that matches the cuts. Similarly, in Fig. 5(c) terms of the Zernike expansion with radial order $n \leq 8$ and azimuthal frequency $m < 8$ have been subtracted from the original height data, revealing the height variations resulting from the eight RK incisions. Higher-order Zernike terms contain an eightfold symmetry that matches the cuts. The terms below the anticipated symmetry of the RK are associated with the refractive power, residual astigmatism, and spherical aberration of the postoperative cornea. Once these terms have been removed, only the artifact resulting from the refractive surgery remains. The six-incision RK artifact shows a peak-to-valley height variation of ~18 μm. The eight-incision RK artifact shows

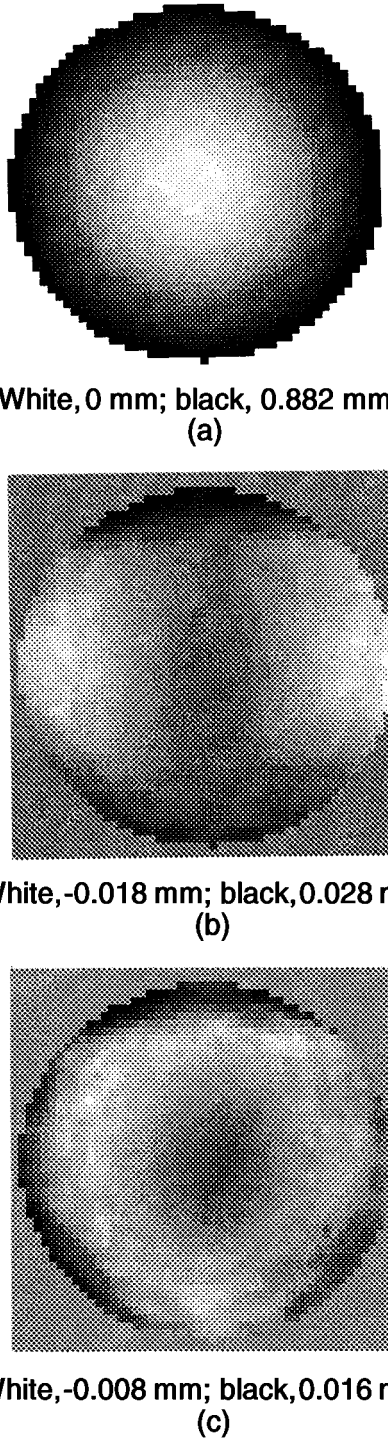

Fig. 2. Height maps of corneal astigmatism: (a) raw height data, (b) raw height data minus the parabolic term, (c) height data of (b) minus the cylindrical term. White represents a high point on the cornea, and black represents a low point. Diameter 7.0 mm.

a peak-to-valley height variation of $\sim 20\ \mu$m. Expansion terms of higher order than the anticipated symmetry of the artifacts can be used to fit these RK artifacts.

5. NUMERICAL ACCURACY

Videokeratoscopes measure corneal surface slope in the meridional direction. Some inaccuracies will result in converting this slope data to height data. Greivenkamp *et al.*[14] have measured the surface height of a variety of toric surfaces on several commercially available videokeratoscopes. The calculated surface heights were compared with the actual heights of the surfaces to determine the accuracy of the videokeratoscope. The error in calculated surface height results from several sources: the lack of azimuthal information about the corneal slope

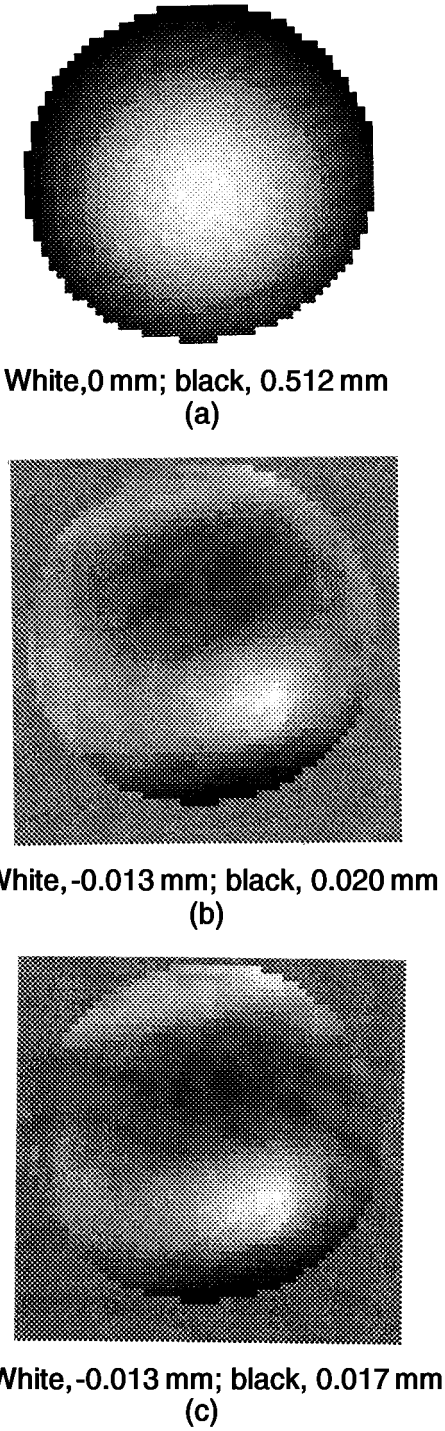

Fig. 3. Height maps of advanced keratoconus: (a) raw height data, (b) raw height data minus the parabolic term, (c) height data of (b) minus the cylindrical term. White represents a high point on the cornea, and black represents a low point. Diameter 5.5 mm.

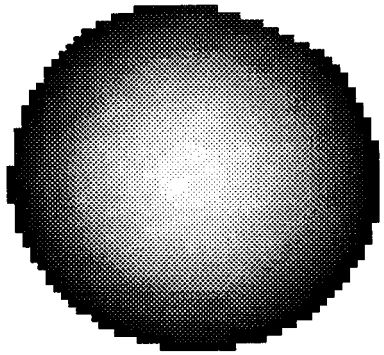

White, 0 mm; black, 1.007 mm
(a)

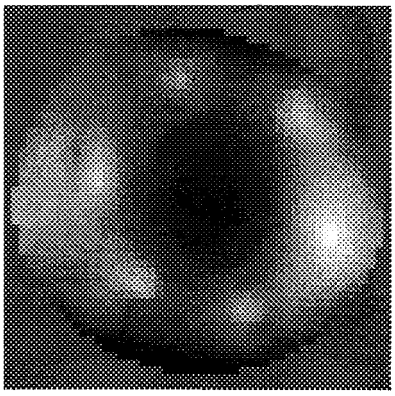

White, -0.047 mm; black, 0.040 mm
(b)

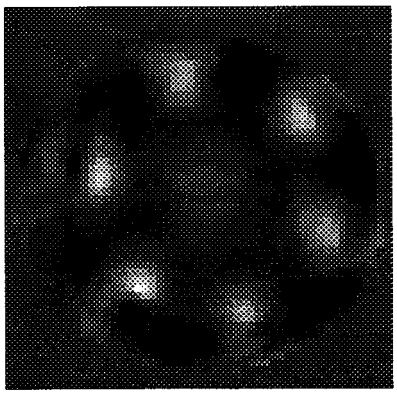

White, -0.027 mm; black, 0.010 mm
(c)

Fig. 4. Height maps of six-incision radial keratotomy: (a) raw height data, (b) raw height data minus the parabolic term, (c) height data of (b) minus the Zernike terms, with $n \leq 6$ and $m < 6$. White represents a high point on the cornea, and black represents a low point. Diameter 8.0 mm.

data, tilt between the optical axis of the cornea and the optical axis of the keratoscope head, and defocus of the corneal image. Under ideal circumstances the rms surface-height errors ranged from 0.7 μm for a 0 D toric up to 4.2 μm for a 7 D toric. In order to determine the accuracy of the Gram–Schmidt orthogonalization routine, we fitted simulated perfect keratographic data sets of 0, 1, 3, 5, and 7 D torics, using the Zernike expansion, and calculated the rms error of the fit. The rms fit error for these five ideal surfaces is less than 0.02 μm for an expansion with radial orders $n \leq 8$ and azimuthal frequencies $m < 8$. This rms fit error is well below the measurement accuracy of the videokeratoscope. In other words, the numerical accuracy of the decomposition methodology outlined here is limited by the measurement device and not by the orthogonalization routine.

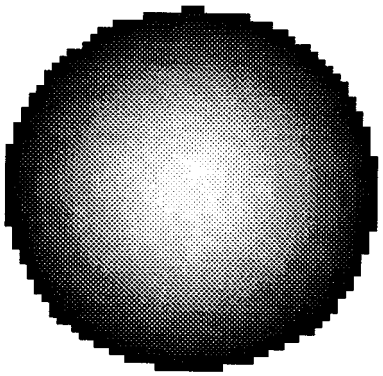

White, 0 mm; black, 0.950 mm
(a)

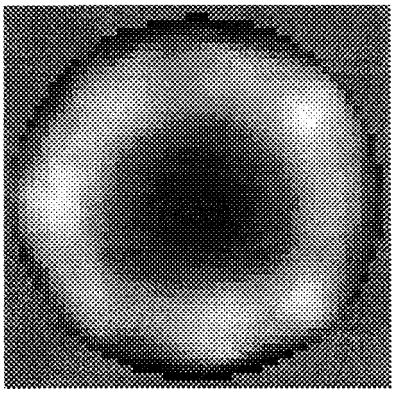

White, -0.020 mm; black, 0.029 mm
(b)

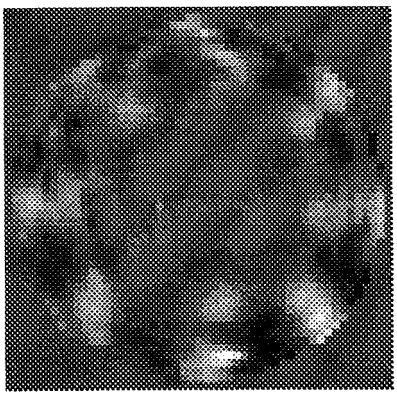

White, -0.010 mm; black, 0.010 mm
(c)

Fig. 5. Height maps of eight-incision radial keratotomy: (a) raw height data, (b) raw height data minus the parabolic term, (c) height data of (b) minus the Zernike terms, with $n \leq 8$ and $m < 8$. White represents a high point on the cornea, and black represents a low point. Diameter 7.6 mm.

Table 1. Actual and Calculated Radii of Curvature in Terms of $R \times R_\perp$ for Several Toric Surfaces

Astigmatism of Toric Surface (D)	Actual	Calculated
0	7.80 mm × 7.80 mm	7.84 mm × 7.81 mm
1	7.80 mm × 7.62 mm	7.89 mm × 7.69 mm
3	7.80 mm × 7.29 mm	7.80 mm × 7.30 mm
5	7.80 mm × 6.99 mm	7.85 mm × 7.03 mm
7	7.80 mm × 6.71 mm	7.85 mm × 6.76 mm

The accuracy of Eqs. (29)–(33) depends on both the accuracy of the videokeratoscope height data and the Zernike expansion coefficients. We have truncated the expressions for spherical and cylindrical radii of curvature and power to keep the equations simple. In deriving these formulas, we find expansion terms containing $\rho^2 = (r/r_{\max})^2$ oriented along and perpendicular to θ_0 (i.e., spherical or cylindrical terms) and compare them with Eq. (27). Equations (29)–(33) contain only the first two spherical terms ($a_{2,0}$ and $a_{4,0}$) and the first two sets of astigmatic terms ($a_{2,2}$, $a_{2,-2}$ and $a_{4,2}$, $a_{4,-2}$). As the order of the expansion is increased, additional terms containing a ρ^2 dependence arise (the next logical terms are $a_{6,0}$ and $a_{6,2}$, $a_{6,-2}$ for the spherical and the cylindrical components, respectively). The accuracy of the radii-of-curvature and the power calculations can be increased by inclusion of these and additional higher-order terms; however, the expressions become cumbersome.

For most corneas the lower-order Zernike polynomial terms carry most of the significant information. The higher-order terms therefore tend to become less reliable as the measurement noise approaches the amount of surface variation represented by these terms. However, for surfaces with significant variations that can be described only by higher-order terms, such as the incision pattern due to an RK procedure, the coefficients for these high-order terms are found to be stable and reliable. As a test, we measured the cornea of an RK patient four times, decomposed the results, and compared the coefficients. All of the corneal height data have the same $r_{\max}$. For all of the coefficients examined (45 terms), the ratio of the mean value to the standard deviation of the coefficient measurements exceeds unity. For polynomial terms representing significant surface variations (such as the eightfold symmetry described above), this signal-to-noise measure of the coefficient quality is on the order of 10:1.

The toric surfaces mentioned above were used to determine the accuracy of the spherical and the astigmatic radii-of-curvature and power calculations. The keratographs of the torics obtained with the TMS-1 were decomposed into a set of Zernike polynomials and values for the radii of curvature calculated with Eqs. (29) and (31). Table 1 shows the actual and the calculated prescriptions of the five toric surfaces in terms of the radius of curvature R along one principal meridian of the toric and the radius of curvature $R_\perp$ along the perpendicular axis. The rms radius error is ~ 50 μm for the five surfaces, which corresponds to a rms power error of less than 0.3 D. The errors produced by Eqs. (29)–(33) are therefore approaching the accuracy level claimed by videokeratoscope manufacturers. If additional accuracy is needed, higher-order terms can be included.

6. CONCLUSION

A technique for analyzing and displaying corneal height data was presented. The height data were decomposed into an orthonormal set of polynomials and related to the Zernike polynomials. The Zernike polynomials provide a numerically stable expansion of corneal height data and contain terms representative of fundamental corneal shapes such as sphere and cylinder. Some previous efforts at decomposing corneal height data use a nonorthogonal expansion such as the Taylor series. The Zernike polynomials have an advantage over the nonorthogonal expansions when high-order fits such as those found in the radial keratotomy examples above are performed. Whereas the Zernike polynomials remain numerically stable, the Taylor series expansion quickly becomes ill-conditioned.[9]

A significant drawback to viewing corneal height data concerns the display of pertinent height data. Small, high-order variations in corneal height are hidden by the spherical and cylindrical components of the cornea. To eliminate this drawback, one can display the height data in stages in order to examine the different components that make up the shape of the cornea. The spherical, cylindrical, and higher-order terms can be individually removed. This decomposition technique has several obvious applications. One application is as a complement to corneal power maps. Surface height provides an easy method of determining contact lens fitting, since the spacing between the base curve of the lens and the cornea can be calculated directly. This process is a generalization of the fluorescein maps routinely used in contact lens evaluation. The height maps also provide information about cone location in keratoconus. Finally, the height maps can be used to evaluate irregularities and asymmetries in radial keratotomy incisions. Height maps can also be applied to optical modeling. The height variations measured on the cornea can be applied to a schematic eye model and the optical effects determined with use of optical ray traces. The height variation in the cornea in the RK examples is ~ 20 μm peak to valley and may have significant optical effects. The RK artifacts generated by this technique also demonstrate that the post-RK cornea has high spots or bumps corresponding to the location of the incisions.

We examined the numerical accuracy of the decomposition and analysis techniques in order to validate the methodology. Commercially available videokeratoscopes have intrinsic error in measuring the surface height of the cornea. These errors arise from necessary assumptions about the alignment of the keratoscope and about the azimuthal slope of the cornea. The fit errors result-

ing from the orthogonalization routine are significantly smaller than the errors produced by the videokeratoscope. Therefore, as future generations of videokeratoscopes improve their height-measuring abilities and as new corneal measurement technologies arise, the methodology outlined here will still be a viable technique for analyzing corneal height data.

We presented several examples of the decomposition-and-display technique in order to introduce and educate the reader to residual height maps. These maps appear vastly different from more-familiar power map displays. With a fundamental understanding of the residual height map displays and a little practice, analyzing these residual height maps will become second nature. The examples of the technique included artifacts such as astigmatism, keratoconus, and radial keratotomy. These analysis techniques can obviously be extended to other procedures such as penetrating keratoplasty and photorefractive keratectomy. With the popularity of refractive surgery ever increasing, eye-care providers and vision scientists need additional tools in order to provide high-quality care for these patients. The Zernike decomposition technique and display methods presented here provide a sophisticated analysis tool to complement current techniques of evaluating the corneal surface.

ACKNOWLEDGMENT

The authors thank Raymond Applegate and his associates for providing some of the vidoekeratographic data presented in this paper.

REFERENCES AND NOTES

1. C. Roberts, "The accuracy of 'power' maps to display curvature data in corneal topography systems," Invest. Ophthalmol. Vis. Sci. **35,** 3525–3532 (1994).
2. R. A. Applegate, H. C. Howland, J. Buettner, A. J. Cottinghan, Jr., R. P. Sharp, and R. W. Yee, "Corneal aberrations before and after radial keratotomy (RK) calculated from videokeratometric measurements," in *Vision Science and Its Applications,* Vol. 2 of 1994 OSA Technical Digest Series (Optical Society of America, Washington, D.C., 1994), pp. 58–61.
3. H. C. Howland, J. Buettner, and R. A. Applegate, "Computation of the shapes of normal corneas and their monochromatic aberrations from videokeratometric measurements," in *Vision Science and Its Applications,* Vol. 2 of 1994 OSA Technical Digest Series (Optical Society of America, Washington, D.C., 1994), pp. 54–57.
4. J. P. Carroll, "A method to describe corneal topography," Optom. Vis. Sci. **71,** 259–264 (1994).
5. S. R. Lange and E. H. Thall, "Interoperative corneal topographic measurement using phase-shifted projected fringe contouring," in *Ophthalmic and Visual Optics,* Vol. 3 of 1992 OSA Technical Digest Series (Optical Society of America, Washington, D.C., 1992), pp. 28–31.
6. R. H. Webb, "Zernike polynomial description of ophthalmic surfaces," in *Ophthalmic and Visual Optics,* Vol. 3 of 1992 OSA Technical Digest Series (Optical Society of America, Washington, D.C., 1992), pp. 38–41.
7. C.-J. Kim and R. R. Shannon, "Catalog of Zernike polynomials," in *Applied Optics and Optical Engineering,* R. R. Shannon and J. Wyant, eds. (Academic, New York, 1992), Vol. 10, pp. 193–221.
8. D. Malacara, "Wavefront fitting with discrete orthogonal polynomials in a units radius circle," Opt. Eng. **29,** 672–675 (1990).
9. J. Y. Wang and D. E. Silva, "Wave-front interpretation with Zernike polynomials," Appl. Opt. **19,** 1510–1518 (1980). *Note:* Eq. (34) should read

$$a_j = \left(b_j - \sum_{k=j+1}^{N} \alpha_{kj} a_k \right) \Big/ \alpha_{jj} .$$

10. E. H. Thall and S. R. Lange, "Preliminary results of a new intraoperative corneal topography technique," J. Cataract Refract. Surg. **19,** 193–197 (1993).
11. G. Arfken, *Mathematical Methods for Physicists* (Academic, New York, 1968).
12. J. D. Gaskill, *Linear Systems, Fourier Transforms, and Optics* (Wiley, New York, 1978), pp. 99–107.
13. Robert Parks, NIST, Gaithersburg, Md. 20899 (personal communication, March 1995).
14. J. E. Greivenkamp, M. D. Mellinger, R. W. Snyder, J. T. Schwiegerling, A. E. Lowman, and J. M. Miller, "Videokeratoscopic measurement of toric surfaces: accuracy analysis of the Computed Anatomy TMS-1, the EyeSys Laboratories Corneal Measurement System, and the Visioptic EH-270," submitted to J. Refract. Corneal Surg.